



**HAL**  
open science

## Generation of acoustic solitary waves in a lattice of Helmholtz resonators

Olivier Richoux, Bruno Lombard, Jean-François Mercier

► **To cite this version:**

Olivier Richoux, Bruno Lombard, Jean-François Mercier. Generation of acoustic solitary waves in a lattice of Helmholtz resonators. *Wave Motion*, 2015, 56, pp.85-99. 10.1016/j.wavemoti.2015.02.005 . hal-01069252

**HAL Id: hal-01069252**

**<https://hal.science/hal-01069252v1>**

Submitted on 30 Sep 2014

**HAL** is a multi-disciplinary open access archive for the deposit and dissemination of scientific research documents, whether they are published or not. The documents may come from teaching and research institutions in France or abroad, or from public or private research centers.

L'archive ouverte pluridisciplinaire **HAL**, est destinée au dépôt et à la diffusion de documents scientifiques de niveau recherche, publiés ou non, émanant des établissements d'enseignement et de recherche français ou étrangers, des laboratoires publics ou privés.

# Generation of acoustic solitary waves in a lattice of Helmholtz resonators

Olivier Richoux<sup>a,\*</sup>, Bruno Lombard<sup>b</sup>, Jean-François Mercier<sup>c</sup>

<sup>a</sup>*LAUM, UMR 6613 CNRS, Université du Maine, 72085 Le Mans, France*

<sup>b</sup>*LMA, CNRS, UPR 7051, Aix-Marseille Université, Centrale Marseille, 13402 Marseille, France*

<sup>c</sup>*POEMS, CNRS/ENSTA/INRIA, UMR 7231, ENSTA ParisTech, 91762 Palaiseau, France*

---

## Abstract

This paper addresses the propagation of high amplitude acoustic pulses through a 1D lattice of Helmholtz resonators connected to a waveguide. Based on the model proposed by Sugimoto (J. Fluid. Mech., 244 (1992), 55-78), a new numerical method is developed to take into account both the nonlinear wave propagation and the different mechanisms of dissipation: the volume attenuation, the linear visco-thermic losses at the walls, and the nonlinear absorption due to the acoustic jet formation in the resonator necks. Good agreement between numerical and experimental results is obtained, highlighting the crucial role of the nonlinear losses. Different kinds of solitary waves are observed experimentally with characteristics depending on the dispersion properties of the lattice.

*Keywords:* nonlinear acoustics, solitary waves, Helmholtz resonator, fractional derivatives, shock-capturing schemes

---

## 1. Introduction

2 The dynamics of nonlinear waves in lattices has been the object of a great  
3 interest in the scientific community. This theme has stimulated researches in

---

\*Corresponding author

*Email addresses:* [olivier.richoux@univ-lemans.fr](mailto:olivier.richoux@univ-lemans.fr) (Olivier Richoux),  
[lombard@lma.cnrs-mrs.fr](mailto:lombard@lma.cnrs-mrs.fr) (Bruno Lombard), [jean-francois.mercier@ensta.fr](mailto:jean-francois.mercier@ensta.fr)  
(Jean-François Mercier)

4 a wide range of areas, including the theory of solitons and the dynamics of  
5 discrete networks. Works have been led in electromagnetism and optics [29],  
6 and numerous physical phenomena have been highlighted, such as dynamical  
7 multistability [63, 25, 36], chaotic phenomena [22, 64], discrete breathers  
8 [34, 6, 20] and solitons or solitary waves [37, 38]; for a review, see [28].  
9 Solitary waves have been observed and studied firstly for surface wave in  
10 shallow water [53]. These waves can propagate without change of shape  
11 and with a velocity depending of their amplitude [50]. This phenomenon  
12 has been studied in many physical systems, for instance in fluid dynamics,  
13 optics, plasma physics. For a review, see [19] and the citations in [14].

14 In the field of acoustics, numerous works have shown the existence of  
15 solitary waves in uniform or inhomogeneous rods [12, 31, 3], periodic chains  
16 of elastics beads [33, 2, 11, 13, 44], periodic structures such as lattices or  
17 crystals [9, 23, 26], elastic layers [32, 41, 42], layered structures coated by  
18 film of soft material [30] and microstructured solids [18]. As we can see, most  
19 studies concern elastic waves in solids. Indeed, only a few works deal with  
20 acoustic waves in fluid, even if experimental observations of solitary waves  
21 have been made in the atmosphere [10, 48, 17] or in the ocean [61, 39, 1].

22 One reason of this lack originates from the fact that the intrinsic disper-  
23 sion of acoustic equations is too low to compete with the nonlinear effects,  
24 preventing from the occurrence of solitons. To observe the latter waves, geo-  
25 metrical dispersion must be introduced. It has been the object of the works  
26 of Sugimoto and his co-authors [59, 56, 58, 60], where the propagation of non-  
27 linear waves was considered in a tube connected to an array of Helmholtz res-  
28 onators. A model incorporating both the nonlinear wave propagation in the  
29 tube and the nonlinear oscillations in the resonators has been proposed. The-  
30 oretical and experimental investigations have shown the existence of acoustic  
31 solitary waves [59].

32 The present study extends the work of Sugimoto. We examine the valid-  
33 ity of his theoretical model to describe the propagation of nonlinear acous-  
34 tic waves in a tunnel with Helmholtz resonators. For this purpose, we de-  
35 velop both a new numerical method and real experiments. Compared with  
36 our original methodology presented in [40], improvements are introduced to  
37 model numerically the attenuation mechanisms. The combination of highly-  
38 accurate numerical simulations and experimental results enables to study  
39 quantitatively the generation of solitary waves, and also to determine the  
40 role of the different physical phenomena (such as the linear and nonlinear  
41 losses) on wave properties.

42 The paper is organized as follows. Section 2 introduces the model of Sugimoto [60]. Section 3 presents the evolution equations. The nonlocal fractional derivatives modeling the viscothermic losses are transformed into a set of memory variables satisfying local-in-time ordinary differential equations. Section 4 details the numerical methods. The coefficients of the memory variables are issued from a new optimization procedure, which ensures the decrease of energy. A splitting strategy is then followed to integrate the evolution equations. Compared with [40], another novelty concerns the integration of a nonlinear differential equation describing the nonlinear losses. Section 5 introduces the experimental setup, the acquisition chain, and some validation tests. Section 6 compares the experimental results and the simulated results, confirming the validity of the theoretical model [56] and the existence of acoustic solitary waves.

## 56 2. Problem statement

### 57 2.1. Configuration

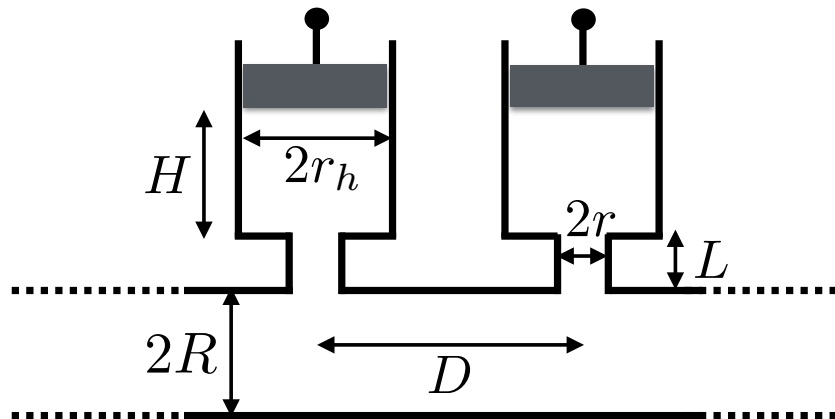


Figure 1: Sketch of the guide connected with Helmholtz resonators.

58 The configuration under study is made up of an air-filled tube connected  
 59 with uniformly distributed cylindrical Helmholtz resonators (figure 1). The  
 60 geometrical parameters are the radius of the guide  $R$ ; the axial spacing be-  
 61 tween resonators  $D$ ; the radius of the neck  $r$ ; the length of the neck  $L$ ; the

62 radius of the cavity  $r_h$ ; and the height of the cavity  $H$ . The cross-sectional  
 63 area of the guide is  $A = \pi R^2$  and that of the neck is  $B = \pi r^2$ , the volume of  
 64 each resonator is  $V = \pi r_h^2 H$ . Corrected lengths are introduced:  $L' = L + 2r$   
 65 accounts for the viscous end corrections, and the corrected length  $L_e = L + \eta$   
 66 accounts for the end corrections at both ends of the neck, where  $\eta \approx 0.82r$   
 67 is determined experimentally [56].

68 The physical parameters are the ratio of specific heats at constant pressure  
 69 and volume  $\gamma$ ; the pressure at equilibrium  $p_0$ ; the density at equilibrium  $\rho_0$ ;  
 70 the Prandtl number  $\text{Pr}$ ; the kinematic viscosity  $\nu$ ; and the ratio of shear  
 71 and bulk viscosities  $\mu_v/\mu$ . The linear sound speed  $a_0$ , the sound diffusivity  
 72  $\nu_d$ , the dissipation in the boundary layer  $C$ , and the characteristic angular  
 73 frequencies of the resonator  $\omega_0$  and  $\omega_e$ , are given by:

$$\begin{aligned}
 a_0 &= \sqrt{\frac{\gamma p_0}{\rho_0}}, & \nu_d &= \nu \left( \frac{4}{3} + \frac{\mu_v}{\mu} + \frac{\gamma - 1}{\text{Pr}} \right), & C &= 1 + \frac{\gamma - 1}{\sqrt{\text{Pr}}}, \\
 \omega_0 &= a_0 \sqrt{\frac{B}{LV}} = a_0 \frac{r}{r_h} \frac{1}{\sqrt{LH}}, & \omega_e &= \sqrt{\frac{L}{L_e}} \omega_0.
 \end{aligned}
 \tag{1}$$

## 74 2.2. Model of Sugimoto

75 Given a characteristic angular frequency  $\omega$ , the main assumptions under-  
 76 lying Sugimoto's model are [56]:

- 77 • low-frequency propagation ( $\omega < \omega^* = \frac{1.84 a_0}{R}$ ), so that only the plane  
 78 mode propagates and the 1D approximation is valid [7];
- 79 • weak acoustic nonlinearity in the tube (small Mach number) [24];
- 80 • continuous distribution of resonators ( $\lambda \gg D$ , where  $\lambda = 2\pi a_0/\omega$ ).

81 The wave fields are split into simple right-going waves (denoted +) and left-  
 82 going waves (denoted -) that do not interact together during their propa-  
 83 gation. The variables are the axial velocity of the gas  $u^\pm$  and the excess  
 84 pressure in the cavity  $p^\pm$ . The excess pressure in the tube is denoted by  $p'^\pm$ .  
 85 In the linear theory, it is related to  $u^\pm$  by

$$p'^\pm = \pm \rho_0 a_0 u^\pm. \tag{2}$$

Each simple wave is modeled by a coupled system of a partial differential equation (PDE) and a ordinary differential equation (ODE):

$$\begin{cases} \frac{\partial u^\pm}{\partial t} + \frac{\partial}{\partial x} \left( \pm a u^\pm + b \frac{(u^\pm)^2}{2} \right) = \pm c \frac{\partial^{-1/2}}{\partial t^{-1/2}} \frac{\partial u^\pm}{\partial x} + d \frac{\partial^2 u^\pm}{\partial x^2} \mp e \frac{\partial p^\pm}{\partial t}, & (3a) \\ \frac{\partial^2 p^\pm}{\partial t^2} + f \frac{\partial^{3/2} p^\pm}{\partial t^{3/2}} + g p^\pm - m \frac{\partial^2 (p^\pm)^2}{\partial t^2} + n \left| \frac{\partial p^\pm}{\partial t} \right| \frac{\partial p^\pm}{\partial t} = \pm h u^\pm, & (3b) \end{cases}$$

86 with the coefficients

$$\begin{aligned} a &= a_0, & b &= \frac{\gamma + 1}{2}, & c &= \frac{C a_0 \sqrt{\nu}}{R^*}, & d &= \frac{\nu_d}{2}, & e &= \frac{V}{2 \rho_0 a_0 A D}, \\ f &= \frac{2 \sqrt{\nu}}{r} \frac{L'}{L_e}, & g &= \omega_e^2, & h &= \omega_e^2 \frac{\gamma p_0}{a_0}, & m &= \frac{\gamma - 1}{2 \gamma p_0}, & n &= \frac{V}{B L_e \rho_0 a_0^2}. \end{aligned} \quad (4)$$

87 The PDE (3a) models nonlinear acoustic waves in the tube (coefficients  $a$   
88 and  $b$ ). Viscous and thermal losses in the boundary layer of the tube are  
89 introduced by the coefficient  $c$  [8]. The diffusivity of sound in the tube is  
90 also introduced by the coefficient  $d$ .

91 The ODE (3b) models the air oscillation in the neck of the resonators  
92 thanks to the coefficients  $f$  and  $g$  [45, 46]. Compared to the ODE used in  
93 [40], the following modifications have been introduced:

- 94 • the natural angular frequency of the resonator  $\omega_0$  has been replaced by  
95 the corrected angular frequency  $\omega_e$  (1),
- 96 •  $f$  has been multiplied by  $L'/L_e$ ,
- 97 • new coefficients  $m$  and  $n$  have been introduced, describing nonlinear  
98 attenuation processes.

99 The coefficient  $m$  models the nonlinearity due to the adiabatic process in  
100 the cavity, whereas the semi-empirical coefficient  $n$  accounts for the jet loss  
101 resulting from the difference in inflow and outflow patterns [56, 60]. As it  
102 will be illustrated later, these nonlinear losses need to be included to get  
103 good agreement with the experimental measurements.

104 The coupling between (3a) and (3b) is done by the coefficients  $e$  and  $h$ . If  
105 the resonators are suppressed ( $H \rightarrow 0$  and thus  $V \rightarrow 0$ ), then the coefficient  
106  $e \rightarrow 0$ : no coupling occurs, and the classical Chester's equation is recovered  
107 [43].

108 Fractional operators of order  $-1/2$  and  $3/2$  are involved in the system (3),  
 109 via the coefficients  $c$  and  $f$ . These operators model the viscothermal losses  
 110 in the tube and in the resonators, respectively proportional to  $1/(i\omega)^{1/2}$  and  
 111  $(i\omega)^{3/2}$  in the frequency domain. In (3a), the Riemann-Liouville fractional  
 112 integral of order  $1/2$  of a causal function  $w(t)$  is defined by

$$\frac{\partial^{-1/2}}{\partial t^{-1/2}} w(t) = \frac{H(t)}{\sqrt{\pi t}} * w = \frac{1}{\sqrt{\pi}} \int_0^t (t - \tau)^{-1/2} w(\tau) d\tau, \quad (5)$$

113 where  $*$  is the convolution product in time, and  $H(t)$  is the Heaviside step  
 114 function [47]. The Caputo fractional derivative of order  $3/2$  in (3b) is ob-  
 115 tained by applying (5) to  $\partial^2 p^\pm / \partial t^2$ .

### 116 2.3. Dispersion regimes

117 Sugimoto's model (3) relies on a low-frequency assumption. In this case,  
 118 the set of discrete Helmholtz resonators separated by portions of tube are  
 119 replaced by a continuous surfacic distribution of resonators. To examine the  
 120 validity of this model in our experimental configuration, one can compare  
 121 the dispersion relations obtained respectively by the continuous model and  
 122 by the discrete one, the latter being deduced from a Floquet-Bloch analysis  
 123 [57].

124 In the linear regime, the lossy continuous model proposed by Sugimoto  
 125 leads to the following dispersion relation [57]:

$$(QD)^2 = \left( 1 - \sqrt{2}(1-i) \frac{C}{R^*} \left( \frac{\nu}{\omega} \right)^{1/2} + i \frac{\nu_d \omega}{a_0^2} \right)^{-1} \left( 1 - \frac{\kappa}{Z_2(\omega)} \right) \left( \frac{\omega D}{a_0} \right)^2, \quad (6)$$

where  $Q$  is the Bloch wave number,  $\kappa = V/(AD)$  and

$$Z_2(\omega) = \left( \frac{\omega}{\omega_e} \right)^2 - 1 + \frac{\sqrt{2}(1-i)}{r} \frac{L'}{L_e} \left( \frac{\nu}{\omega_e} \right)^{1/2} \left( \frac{\omega}{\omega_e} \right)^{3/2}.$$

126 On the contrary, the dispersion relation of the discrete model writes [52]

$$\cos QD = \cos(kD) + \frac{U(k)}{2k} \sin(kD), \quad (7)$$

127 where  $k = \omega/a_0$  is the wave number and  $U(k)$  is the equivalent potential of  
 128 the Helmholtz resonators given by

$$U(k) = \frac{B}{A k} \frac{\tan(k L_e) + \alpha \tan(k H)}{1 - \alpha \tan(k L_e) \tan(k H)}, \quad (8)$$

129 with  $\alpha = (r_h/r)^2$ . The losses in the waveguide and resonators are modeled  
 130 by introducing an imaginary part in the wavenumber  $k$  as presented in [57].  
 131 Results from equations (6) and (7) will be compared in section 5.3.

### 132 3. Evolution equations

#### 133 3.1. Diffusive approximation

134 The fractional integral (5) is non local in time and relies on the full history  
 135 of  $w(t)$ , which is numerically memory-consuming. An alternative approach  
 136 is based on a diffusive representation of fractional derivatives, and then on  
 137 its approximation. This method has already been presented in [40] and we  
 138 just recall the main steps: following [15], equation (5) is recast as

$$\frac{\partial^{-1/2}}{\partial t^{-1/2}} w(t) = \int_0^{+\infty} \phi(t, \theta) d\theta, \quad (9)$$

139 where the diffusive variable  $\phi$  satisfies the local-in-time ordinary differential  
 140 equation

$$\begin{cases} \frac{\partial \phi}{\partial t} = -\theta^2 \phi + \frac{2}{\pi} w, \\ \phi(0, \theta) = 0. \end{cases} \quad (10)$$

141 To approximate the integral (9), a quadrature formula on  $N_q$  points is used,  
 142 with weights  $\mu_\ell$  and nodes  $\theta_\ell$ :

$$\frac{\partial^{-1/2}}{\partial t^{-1/2}} w(t) \simeq \sum_{\ell=1}^{N_q} \mu_\ell \phi_\ell(t), \quad (11)$$

143 where the diffusive variables  $\phi_\ell(t) = \phi(t, \theta_\ell)$  satisfy the ODE (10). Similarly,  
 144 the derivative of order 3/2 is written

$$\frac{\partial^{3/2}}{\partial t^{3/2}} w(t) \simeq \sum_{\ell=1}^{N_q} \mu_\ell \left( -\theta_\ell^2 \xi_\ell + \frac{2}{\pi} \frac{dw}{dt} \right), \quad (12)$$

145 where the  $\xi_\ell(t) = \xi(t, \theta_\ell)$  satisfy the ODE

$$\begin{cases} \frac{\partial \xi}{\partial t} = -\theta^2 \xi + \frac{2}{\pi} \frac{dw}{dt}, \\ \xi(0, \theta) = 0. \end{cases} \quad (13)$$

146 The determination of weights and nodes  $\mu_\ell$  and  $\theta_\ell$  is discussed in section 4.1.



147 *3.2. First-order systems*

148 Equations (3), (11), (10), (12) and (13) governing the evolution of right-  
 149 going and left-going simple waves are put together. One obtains two first-order  
 150 systems

$$\left\{ \begin{array}{l} \frac{\partial u^\pm}{\partial t} + \frac{\partial}{\partial x} \left( \pm a u^\pm + b \frac{(u^\pm)^2}{2} \right) = \pm c \sum_{\ell=1}^{N_q} \mu_\ell \phi_\ell^\pm + d \frac{\partial^2 u}{\partial x^2} \mp e q^\pm, \\ \frac{\partial p^\pm}{\partial t} = q^\pm, \\ \frac{\partial q^\pm}{\partial t} = \frac{1}{1 - 2mp^\pm} \left( \pm h u^\pm - g p^\pm - f \sum_{\ell=1}^{N_q} \mu_\ell \left( -\theta_\ell^2 \xi_\ell^\pm + \frac{2}{\pi} q^\pm \right) + 2m(q^\pm)^2 - n|q^\pm|q^\pm \right), \\ \frac{\partial \phi_\ell^\pm}{\partial t} - \frac{2}{\pi} \frac{\partial u^\pm}{\partial x} = -\theta_\ell^2 \phi_\ell^\pm, \quad \ell = 1 \cdots N_q, \\ \frac{\partial \xi_\ell^\pm}{\partial t} = -\theta_\ell^2 \xi_\ell^\pm + \frac{2}{\pi} q^\pm, \quad \ell = 1 \cdots N_q, \end{array} \right. \quad (14)$$

151 with null initial conditions. A source term at  $x = 0$  models the acoustic  
 152 source of right-going wave

$$u^+(0, t) = s(t). \quad (15)$$

153 The rigid end of the tube is modeled by Dirichlet conditions on the velocity

$$u^-(L, t) = -u^+(L, t), \quad (16)$$

154 hence  $u^+(L, t)$  acts as a source for the system of left-going waves. In the third  
 155 equation of (14), a division by  $1 - 2mp^\pm$  occurs. In practice, this terms does  
 156 not vanish: in the low-frequency regime, one has from (3b) that  $g p^\pm \approx h u^\pm$   
 157 which leads to  $p^\pm/p_0 \approx \gamma u^\pm/a_0$ . From the definition of  $m$  in (4), it follows  
 158 that

$$2mp^\pm \approx (\gamma - 1) \frac{u^\pm}{a_0}, \quad (17)$$

159 which is lower than 1 under the hypothesis of weak nonlinearity ( $|u^\pm| \ll a_0$ ).

160 The  $(3 + 2N_q)$  unknowns for each simple waves are gathered in the two  
 161 vectors

$$\mathbf{U}^\pm = \left( u^\pm, p^\pm, q^\pm, \phi_1^\pm, \dots, \phi_{N_q}^\pm, \xi_1^\pm, \dots, \xi_{N_q}^\pm \right)^T. \quad (18)$$

162 Then the nonlinear systems (14) can be written in the form

$$\frac{\partial}{\partial t} \mathbf{U}^\pm + \frac{\partial}{\partial x} \mathbf{F}^\pm(\mathbf{U}^\pm) = \mathbf{G} \frac{\partial^2}{\partial x^2} \mathbf{U}^\pm + \mathbf{S}^\pm(\mathbf{U}^\pm), \quad (19)$$

163 where  $\mathbf{F}^\pm$  are the flux functions

$$\mathbf{F}^\pm = \left( \pm a u^\pm + b \frac{(u^\pm)^2}{2}, 0, 0, -\frac{2}{\pi} u^\pm, \dots, -\frac{2}{\pi} u^\pm, 0, \dots, 0 \right)^T. \quad (20)$$

164 The Jacobian matrices  $\frac{\partial \mathbf{F}^\pm}{\partial \mathbf{U}^\pm}$  in (20) are diagonalizable with real eigenvalues:  
 165  $\pm a + b u^\pm$ , and 0 with multiplicity  $2 N_q + 2$ , which ensures propagation with  
 166 finite velocity. These eigenvalues do not depend on the quadrature coeffi-  
 167 cients  $\mu_\ell$  and  $\theta_\ell$ . The diagonal matrix  $\mathbf{G} = \text{diag}(d, 0, \dots, 0)$  incorporates  
 168 the volume attenuation. Lastly,  $\mathbf{S}^\pm$  are the source terms

$$\mathbf{S}^\pm = \begin{pmatrix} \pm c \sum_{\ell=1}^N \mu_\ell \phi_\ell^\pm \mp e q^\pm \\ q^\pm \\ \frac{1}{1 - 2mp^\pm} \left( \pm h u^\pm - g p^\pm - f \sum_{\ell=1}^N \mu_\ell \left( -\theta_\ell^2 \xi_\ell^\pm + \frac{2}{\pi} q^\pm \right) + 2m(q^\pm)^2 - n|q^\pm|q^\pm \right) \\ -\theta_\ell^2 \phi_\ell^\pm, \quad \ell = 1 \dots N_q \\ -\theta_\ell^2 \xi_\ell + \frac{2}{\pi} q^\pm, \quad \ell = 1 \dots N_q \end{pmatrix}. \quad (21)$$

169 As soon as  $m \neq 0$  and  $n \neq 0$ ,  $\mathbf{S}^\pm(\mathbf{U}^\pm)$  is no longer a linear operator ( $m =$

170  $0 = n$  has been considered in [40]). The Jacobian matrices  $\mathbf{T}^\pm = \frac{\partial \mathcal{S}^\pm}{\partial \mathbf{U}^\pm}$  are

$$\mathbf{T}^\pm = \begin{pmatrix} 0 & 0 & \mp e & \pm c \mu_1 & \cdots & \pm c \mu_N & 0 & \cdots & 0 \\ 0 & 0 & 1 & 0 & \cdots & 0 & 0 & \cdots & 0 \\ \frac{\pm h}{\Delta^\pm} & -\frac{g}{(\Delta^\pm)^2} & T_{22}^\pm & 0 & \cdots & 0 & \frac{f}{\Delta^\pm} \mu_1 \theta_1^2 & \cdots & \frac{f}{\Delta^\pm} \mu_N \theta_N^2 \\ 0 & 0 & 0 & -\theta_1^2 & & & & & \\ \vdots & \vdots & \vdots & & \ddots & & & & \\ 0 & 0 & 0 & & & -\theta_N^2 & & & \\ 0 & 0 & \frac{2}{\pi} & & & & -\theta_1^2 & & \\ \vdots & \vdots & \vdots & & & & & \ddots & \\ 0 & 0 & \frac{2}{\pi} & & & & & & -\theta_N^2 \end{pmatrix}, \quad (22)$$

171 with

$$\Delta^\pm = 1 - 2mp^\pm, \quad T_{22}^\pm = \frac{1}{\Delta^\pm} \left( 4mq^\pm - 2n|q^\pm| - \frac{2}{\pi} f \sum_{\ell=1}^{N_q} \mu_\ell \right). \quad (23)$$

## 172 4. Numerical methods

### 173 4.1. Quadrature coefficients

174 In [40], a detailed discussion on the possible strategies to compute the  
175  $2N_q$  quadrature coefficients  $\mu_\ell$  and  $\theta_\ell$  in (21) has been proposed, and a  
176 linear optimization was preferred. The nodes  $\theta_\ell$  were distributed linearly on  
177 a logarithmic scale on the frequency range of interest, and then the weights  
178 were determined by a simple least-squares method. One drawback is that  
179 negative weights  $\mu_\ell$  may be obtained, which may yield a non-physical increase  
180 of energy [4].

181 Here we improve the optimization procedure to get positive weights  $\mu_\ell$ .  
182 Dispersion analysis shows that the original model of Sugimoto (3) and its  
183 diffusive counterpart (14) differ only in their symbols

$$\begin{cases} \chi(\omega) = (i\omega)^{-1/2}, \\ \tilde{\chi}(\omega) = \frac{2}{\pi} \sum_{\ell=1}^{N_q} \frac{\mu_\ell}{\theta_\ell^2 + i\omega}. \end{cases} \quad (24)$$

184 For a given number  $K_q$  of angular frequencies  $\omega_k$ , one introduces the objective  
 185 function

$$\mathcal{J}(\{(\mu_\ell, \theta_\ell)\}_\ell; N_q, K_q) = \sum_{k=1}^{K_q} \left| \frac{\tilde{\chi}(\omega_k)}{\chi(\omega_k)} - 1 \right|^2 = \sum_{k=1}^{K_q} \left| \frac{2}{\pi} \sum_{\ell=1}^{N_q} \mu_\ell \frac{(i\omega_k)^{1/2}}{\theta_\ell^2 + i\omega_k} - 1 \right|^2 \quad (25)$$

186 to be minimized w.r.t parameters  $\{(\mu_\ell, \theta_\ell)\}_\ell$  for  $\ell = 1, \dots, N_q$ . A nonlinear  
 187 optimization with the positivity constraints  $\mu_\ell \geq 0$  and  $\theta_\ell \geq 0$  is chosen  
 188 for this purpose. The additional constraint  $\theta_\ell \leq \theta_{\max}$  is also introduced to  
 189 avoid the algorithm to diverge. These  $3N_q$  constraints can be relaxed by  
 190 setting  $\mu_\ell = \mu_\ell'^2$  and  $\theta_\ell = \theta_\ell'^2$  and solving the following problem with only  
 191  $N_q$  constraints

$$\min_{\{(\theta_\ell', \mu_\ell')\}_\ell} \mathcal{J}(\{(\mu_\ell'^2, \theta_\ell'^2)\}_\ell; N_q, K_q) \quad \text{with } \theta_\ell'^2 \leq \theta_{\max} \text{ for } \ell = 1, \dots, N_q. \quad (26)$$

192 As problem (26) is nonlinear and non-quadratic w.r.t. nodes  $\theta_\ell'$ , we implement  
 193 the algorithm SolvOpt [27, 49] based on the iterative Shor's method [54].  
 194 Initial values used in the algorithm must be chosen with care; for this purpose  
 195 we propose to use the coefficients obtained by the modified Jacobi approach  
 196 [5]: see method 3 of [40]. Finally, the angular frequencies  $\omega_k$  for  $k = 1, \dots, K_q$   
 197 in (25) are chosen linearly on a logarithmic scale over a given optimization  
 198 band  $[\omega_{\min}, \omega_{\max}]$ , i.e.

$$\omega_k = \omega_{\min} \left( \frac{\omega_{\max}}{\omega_{\min}} \right)^{\frac{k-1}{K_q-1}}. \quad (27)$$

199 The choice of  $\omega_{\min}$  and  $\omega_{\max}$  depends on the configuration under study (tube  
 200 alone or coupled system with resonators) and has been detailed in [40]. Be-  
 201 sides the positivity of the quadrature coefficients, a great improvement of  
 202 accuracy is observed numerically when using the nonlinear optimization de-  
 203 scribed above.

#### 204 4.2. Numerical scheme

205 In order to integrate the systems (19), a grid is introduced with a uniform  
 206 spatial mesh size  $\Delta x = L/N_x$  and a variable time step  $\Delta t_n$ . The approxi-  
 207 mation of the exact solution  $\mathbf{U}^\pm(x_j = j \Delta x, t_n = t_{n-1} + \Delta t_{n-1})$  is denoted  
 208 by  $\mathbf{U}_j^{n\pm}$ . A splitting strategy is followed here, ensuring both simplicity and

209 efficiency. Instead of integrating the original equations (19), propagative  
 210 equations

$$\frac{\partial}{\partial t} \mathbf{U}^\pm + \frac{\partial}{\partial x} \mathbf{F}^\pm(\mathbf{U}^\pm) = \mathbf{G} \frac{\partial^2}{\partial x^2} \mathbf{U}^\pm \quad (28)$$

211 and forcing equations

$$\frac{\partial}{\partial t} \mathbf{U}^\pm = \mathbf{S}^\pm(\mathbf{U}^\pm) \quad (29)$$

212 are solved successively. The discrete operators to solve (28) and (29) are  
 213 denoted by  $\mathbf{H}_a^\pm$  and  $\mathbf{H}_b^\pm$ , respectively. Strang splitting [62] is then used  
 214 between  $t_n$  and  $t_{n+1}$ , solving successively (28) and (29) with adequate time  
 215 increments:

$$\begin{aligned} \bullet \quad \mathbf{U}_j^{(1)\pm} &= \mathbf{H}_b^\pm\left(\frac{\Delta t_n}{2}\right) \mathbf{U}_j^{n\pm}, \\ \bullet \quad \mathbf{U}_j^{(2)\pm} &= \mathbf{H}_a^\pm(\Delta t_n) \mathbf{U}_j^{(1)\pm}, \\ \bullet \quad \mathbf{U}_j^{(n+1)\pm} &= \mathbf{H}_b^\pm\left(\frac{\Delta t_n}{2}\right) \mathbf{U}_j^{(2)\pm}. \end{aligned} \quad (30)$$

216 Provided that  $\mathbf{H}_a^\pm$  and  $\mathbf{H}_b^\pm$  are second-order accurate and stable operators,  
 217 the time-marching (30) gives second-order accurate approximations of the  
 218 original equations (19).

219 As explained in [40], the propagative equation (28) is solved by a standard  
 220 second-order TVD scheme for nonlinear hyperbolic PDE [35] combined with  
 221 a centered finite-difference approximation. The discrete operator  $\mathbf{H}_a$  is stable  
 222 under a usual CFL condition.

223 Contrary to [40] where  $\mathbf{S}^\pm$  was a constant linear operator, the forcing  
 224 equations (29) can no longer be solved exactly. Here, they are solved by a  
 225 second-order implicit trapezoidal method [62]

$$\mathbf{U}^{(n+1)\pm} = \mathbf{U}^{n\pm} + \frac{\tau_n}{2} (\mathbf{S}^\pm(\mathbf{U}^{n\pm})) + \mathbf{S}^\pm(\mathbf{U}^{(n+1)\pm}), \quad (31)$$

226 with  $\tau_n = \Delta t_n/2$ . The nonlinear systems (31) are solved iteratively by the  
 227 Newton-Raphson method. In practice, a single iteration is accurate enough.  
 228 Linearizing the equations and using the Jacobian (22), the discrete operator  
 229  $\mathbf{H}_b^\pm$  recovers the semi-implicit trapezoidal scheme

$$\mathbf{U}^{(n+1)\pm} = \mathbf{U}^{n\pm} + \tau_n \left( \mathbf{I} - \frac{\tau_n}{2} \mathbf{T}^{n\pm} \right)^{-1} \mathbf{S}^\pm(\mathbf{U}^{n\pm}), \quad (32)$$

230 which is unconditionnally stable.

231 Once time-marching is completed, the source terms (15) and (16) are  
 232 updated at the grid nodes 0 (for the right-going wave) and  $N_x$  (for the left-  
 233 going wave). The forcing term  $s(t_n)$  in (15) is obtained from (2) and from  
 234 the pressure  $p'(0, t_n)$  measured experimentally by the first microphone: see  
 235 section 5 for details on that topic.

## 236 5. Experimental set-up and validation

### 237 5.1. Lattice sample

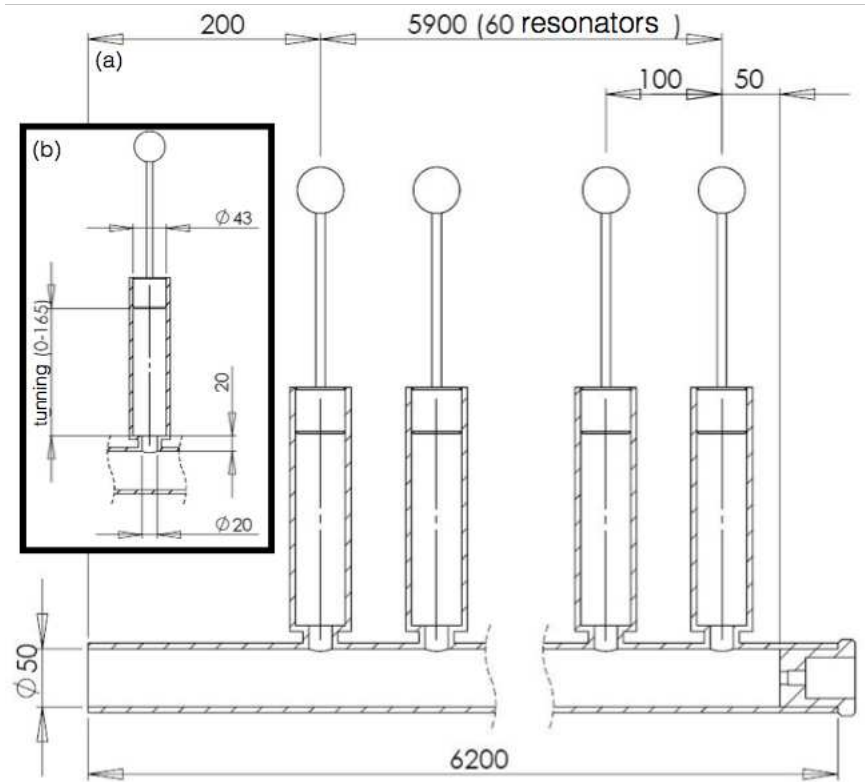


Figure 2: experimental set-up; all the dimensions are detailed in mm. (a): description of the Helmholtz resonators lattice. (b): description of one Helmholtz resonator.

238 The experimental set-up shown in figure 2-(a) consists in a 6.2 m long  
 239 cylindrical waveguide connected to an array of 60 Helmholtz resonators pe-  
 240 riodically distributed. All the cavities have the same height  $H$ , which may

241 varies between 0 and  $H_{max} = 0.165$  m, as described in figure 2-(b). The  
 242 physical and geometrical parameters are given in table 1. The physical data  
 243 correspond to air at 15 °C.

$\gamma$	$p_0$ (Pa)	$\rho_0$ (kg/m <sup>3</sup> )	$Pr$	$\nu$ (m <sup>2</sup> /s)	$\mu_v/\mu$
1.403	10 <sup>5</sup>	1.177	0.708	1.57 10 <sup>-5</sup>	0.60
$R$ (m)	$D$ (m)	$r$ (m)	$L$ (m)	$r_h$ (m)	$H_{max}$ (m)
0.025	0.1	0.01	0.02	0.0215	0.165

Table 1: physical parameters of air at 15 °C, and geometrical data.

244 The first resonator lies 0.2 m after the beginning of the tube. The end of  
 245 the lattice is closed by a rigid cork located at  $D/2$  after the last resonator.  
 246 Then, the waves impinging the lattice end are reflected and travel in the  
 247 opposite direction (keeping the cell length constant) into the lattice, allowing  
 248 to increase the lattice length from 6 m to 12 m. Numerical modeling of this  
 249 configuration amounts to solve (3) by considering a 0.2 m long waveguide  
 250 with no resonator, connected to a 5.95 m long lattice of resonators closed by  
 251 a rigid end, in accordance with the experimental set-up.

252 A second experimental system, consisting in a waveguide with no array  
 253 of resonator, is used in section 5.4 to highlight the influence of the Helmholtz  
 254 resonators in the nonlinear process. This waveguide has exactly the same  
 255 features than the previous one. Numerical modeling of this configuration  
 256 amounts to solve (3a) on a 6.15 m long waveguide closed by a rigid end, with  
 257  $e = 0$ .

## 258 5.2. Source and acquisition

259 The input signal is generated by the explosion of a balloon. The latter  
 260 is introduced into a 20 cm long waveguide connected to the main tube and  
 261 is inflated until its explosion. The shape of the generated impulsion (width  
 262 and amplitude) depends on the balloon length at the explosion time, varying  
 263 slightly from one experiment to the other.

264 The excess pressure  $p' = p'^+ + p'^-$  is measured with 3 PCB 106B micro-  
 265 phones. They are located at the beginning of the system (20 cm before the  
 266 first resonator) and at 2 different positions into the lattice, depending on the  
 267 experiment. The sensibility of the microphones is 0.045 V/kPa, and a PCB  
 268 441A101 conditioning amplifier is used for each of them. The acquisition is  
 269 made by a National Instrument BNC 2110 card with a sample frequency of  
 270 250 kHz, connected to a computer.

271 The input signal shown in the figure 3-(a) can be described by a gate-  
 272 signal with a high amplitude around 30 kPa, and a width around 1.5 ms  
 273 with the presence of a tail caused by reflexion at the end of the source tube.  
 274 The initial excess pressure consists of a compression wave. The figure 3-(b)  
 275 shows the spectrum of the input signal and points out that the frequency  
 276 range excited by the source is mostly included in  $[0 - 650]$  Hz. This input  
 277 signal, generated by the balloon explosion, is measured at each experiment.  
 278 It is then injected in the numerical scheme and acts as a forcing term  $s$ : see  
 279 section 4.2. In other words, our resolution method requires only the input  
 280 data signal as initial conditions to solve the system (3). It is an important  
 281 difference with the resolution method in [60] which requires the fitting of the  
 282 experimental signal after some distance of propagation.

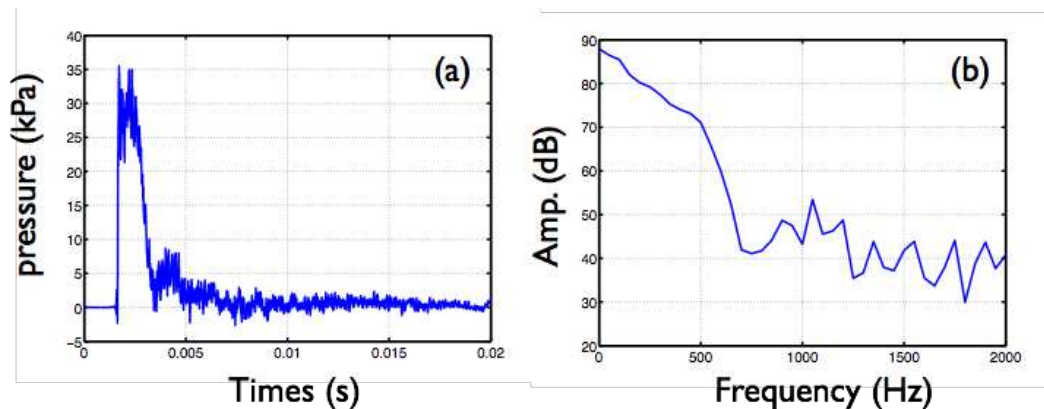


Figure 3: acoustic source measured at the entry of the tube. (a): time history of the excess pressure  $p'^+(0, t)$ . (b): Fourier transform of the signal.

### 283 5.3. Linear dispersion in a Helmholtz resonator lattice

284 The goal of this section is to examine the validity of the model (3) to  
 285 describe the experimental configuration under study. For this purpose, figure  
 286 4 compares the dispersion curves obtained with the continuous description of  
 287 resonators (6) and with the discrete description (7). Three different heights of  
 288 resonators are considered:  $H = 16.5$  cm ( $f_0 = 345$  Hz),  $H = 7$  cm ( $f_0 = 586$   
 289 Hz), and  $H = 2$  cm ( $f_0 = 1027$  Hz). In each case,  $f_0 = \omega_0/(2\pi)$  is the  
 290 resonance frequency of the Helmholtz resonators (1).



291 Good agreement between these two families of dispersion curves is ob-  
 292 tained on a large frequency domain, up to the Bragg band gap at 1800  
 293 Hz. Because of the continuous approximation, equation (6) cannot predict  
 294 the Bragg band gap due to the lattice periodicity. However, the first hy-  
 295 bridization band gap (due to Helmholtz resonance) is well described by the  
 296 continuous model.

297 A second observation deduced from figure 4 concerns the dispersive be-  
 298 havior of the medium under study. Recall that the upper limit of the source  
 299 frequency range  $f_{\max}$  is around 650 Hz. If  $f_0 \gg f_{\max}$  (i.e.  $H = 2$  cm),  
 300 we observe a linear frequency dependance of  $QD$  in  $[0, f_{\max}]$ , which implies  
 301 that the dispersion is weak (figure 4-(c)). On the contrary, when  $f_0$  lies in  
 302 the source frequency range (figure 4-(a) for  $H = 16.5$  cm and figure (4b) for  
 303  $H = 7$  cm), the dispersion is strong. This impacts strongly the shape of the  
 304 waves, as detailed in section 6.4.

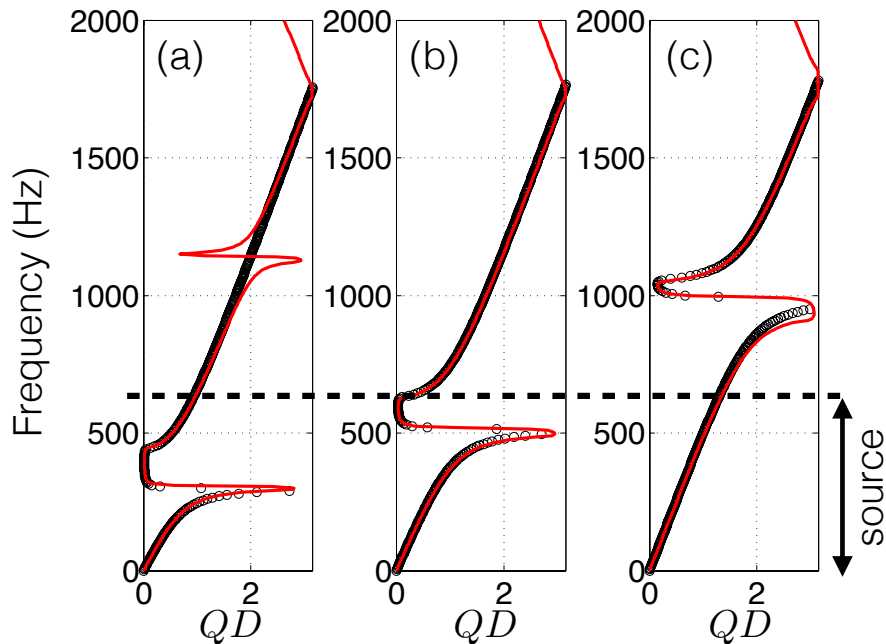


Figure 4: dispersion relation of an array of Helmholtz resonators for  $H = 16.5$  cm (a),  $H = 7$  cm (b) and  $H = 2$  cm (c). The open circles correspond to the continuous model (6). The continuous red line corresponds to the discrete model (7).

305 *5.4. Tube without resonators*

306 Before considering the interaction of waves with the lattice of resonators,  
 307 we consider the simple case of a uniform tube. Figure 5 shows the profiles  
 308 of the measured and simulated excess pressure  $p'/p_s$  at the position  $x = 6.15$   
 309 m in a waveguide without resonator, where  $p_s$  is the magnitude of the input  
 310 signal. The blue and red lines correspond to the simulated and experimental  
 311 results, respectively. The initial pressure wave has evolved to a triangular  
 312 shape wave during the propagation, due to a well-known nonlinear process  
 313 [24, 43].

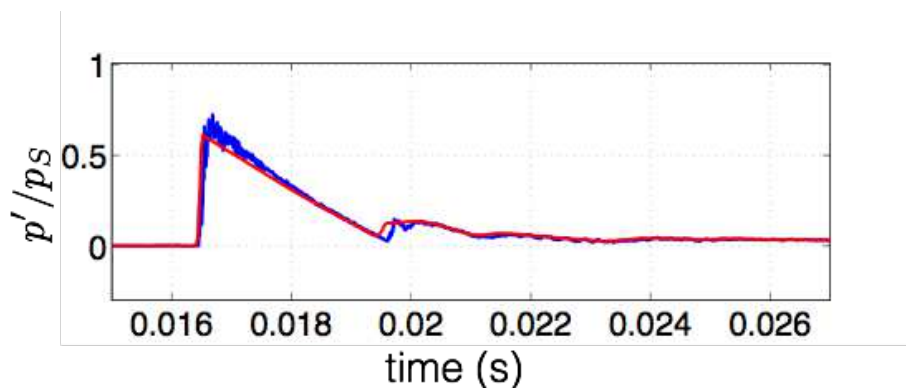


Figure 5: time history of the excess pressure  $p'/p_s$  in a tube with no array of resonators, at  $x = 6.15$  m. The blue and red lines represent the experimental and simulated profiles, respectively.

314 The good agreement between the simulated and measured pressure high-  
 315 lights the validity of the lossy nonlinear model for the waveguide propagation  
 316 described by the equation (3a) where the coupling term with the resonators  
 317 is canceled. The model describing the losses in the waveguide propagation by  
 318 fractional derivatives is verified by this comparison and will not be discussed  
 319 further. Note lastly that the volume attenuation and the viscothermic losses  
 320 in the tube are insufficient to prevent from the occurrence of shocks [55].

321 **6. Experiments in a tube with resonators**

322 *6.1. Existence of solitary waves*

323 Figure 6 presents the experimental and simulated temporal profiles  $p'/p_s$   
 324 at  $x = 2.1$  m, in a waveguide connected to an array of Helmholtz resonators.

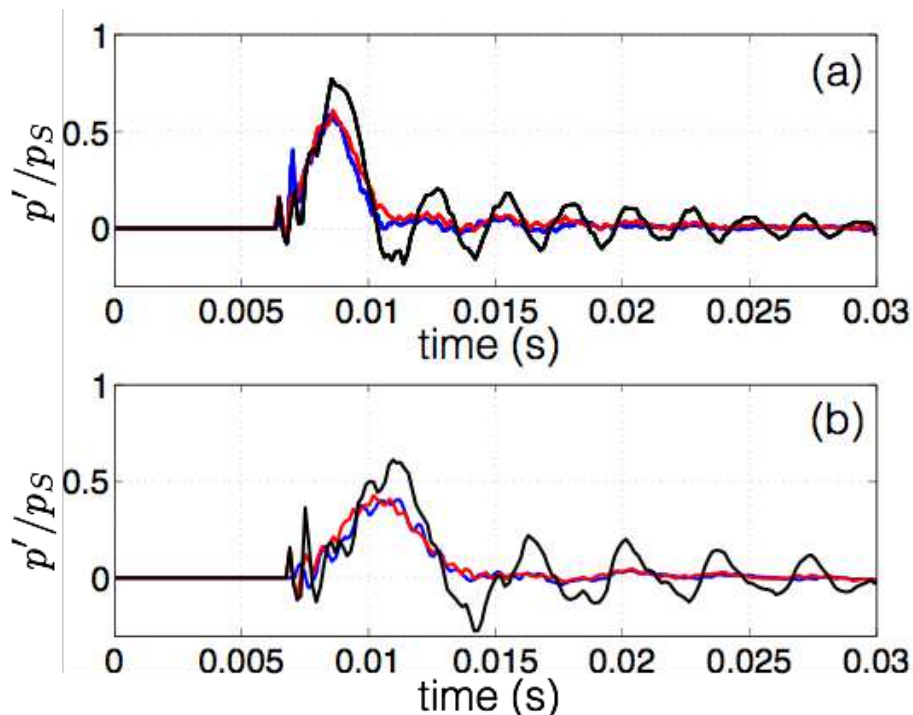


Figure 6: time history of the excess pressure  $p'/p_s$  at  $x = 2.1$  m in a tube with an array of resonators. The heights of resonators are:  $H = 7$  cm (a),  $H = 13$  cm (b). The blue line represents the experimental pressure. The red and black lines represent the simulated pressure, with (red) or without (black) nonlinear losses.

325 The heights of resonators are  $H = 7$  cm (figure 6-(a)) and  $H = 13$  cm (figure  
 326 6-(b)), respectively. In the case  $H = 7$  cm (resp.  $H = 13$  cm), the resonance  
 327 frequency  $f_0$  of the Helmholtz resonators is  $f_0 \simeq 586$  Hz (resp.  $f_0 \simeq 414$   
 328 Hz). The blue line depicts the experimental results. The red line depicts the  
 329 numerical results where all the physical phenomena are incorporated, leading  
 330 to the full system (3). The black line depicts the numerical solution obtained  
 331 without incorporating the nonlinear losses in the resonator necks:  $m = n = 0$   
 332 in (3b).

333 Unlike the waveguide without resonators, where a triangular wave is ob-  
 334 tained (figure 5), the lattice produces a wave with a smooth and symmetrical  
 335 shape (figure 6). This constitutes a signature of solitary waves.

336 Good agreement between experimental and simulated waves is obtained

337 when the nonlinear losses are taken into account. On the contrary, the lin-  
338 ear viscothermic losses alone are insufficient to predict the right amplitude,  
339 which is overestimated compared to the experimental results. Moreover, spu-  
340 rious oscillations are observed in the linear case, that are suppressed when  
341 nonlinear losses are incorporated.

342 In addition, the comparison between the heights  $H = 7$  cm (figure 6-(a))  
343 and  $H = 13$  cm (figure 6-(b)) highlights the influence of the resonators on the  
344 evolution of the pulse. The solitary wave being the result of a competition  
345 between the nonlinearity and the dispersion in the media, it is very sensitive  
346 to the cavity length. The decrease of the Helmholtz resonance frequency  
347 leads to an increase of the wave attenuation, an increase of the pulse width,  
348 and a decrease of the wave celerity. These results corroborate the theoretical  
349 analysis performed in [60] and confirm the existence of an acoustic solitary  
350 wave.

## 351 *6.2. Spatio-temporal evolution*

352 In this section, we illustrate the evolution of solitary waves during their  
353 propagation, in the case  $H = 13$  cm. Figure 7 displays the experimental  
354 results (top panel) and the simulated results with nonlinear lossy attenuation  
355 (bottom panel), in the space  $\times$  time plane.

356 Experimentally (figure 7-(a)), the signals have been recorded at 15 dif-  
357 ferent positions of microphones regularly spaced, from 0.2 m to 4.4 m inside  
358 the lattice with a spacing 0.3 m. Since only two microphones were available,  
359 acquisition was performed during 8 successive experiments, the pair of micro-  
360 phones being successively shifted. A new source was used in each experiment,  
361 leading to small deviations from one experiment to the other. These 8 sources  
362 were used as initial data for the corresponding numerical simulations. For  
363 both experiments and simulations, we present the ratio between the excess  
364 pressure in the waveguide and the source amplitude  $p'/p_s$ .

365 Figure 7 clearly shows the propagation of a solitary wave without change  
366 of shape and with a constant velocity characterized by a constant slope in the  
367 space  $\times$  time plane, both experimentally and numerically. The symmetry of  
368 figure 7 with respect to time  $t = 29$  ms illustrates the reflexion of the solitary  
369 wave at the closed end of the tube. A second reflexion at the opposite closed  
370 end is visible in the experimental case, but it is not simulated numerically.  
371 The experimental and simulated results are in good agreement, for both the  
372 shape and the velocity of the waves.

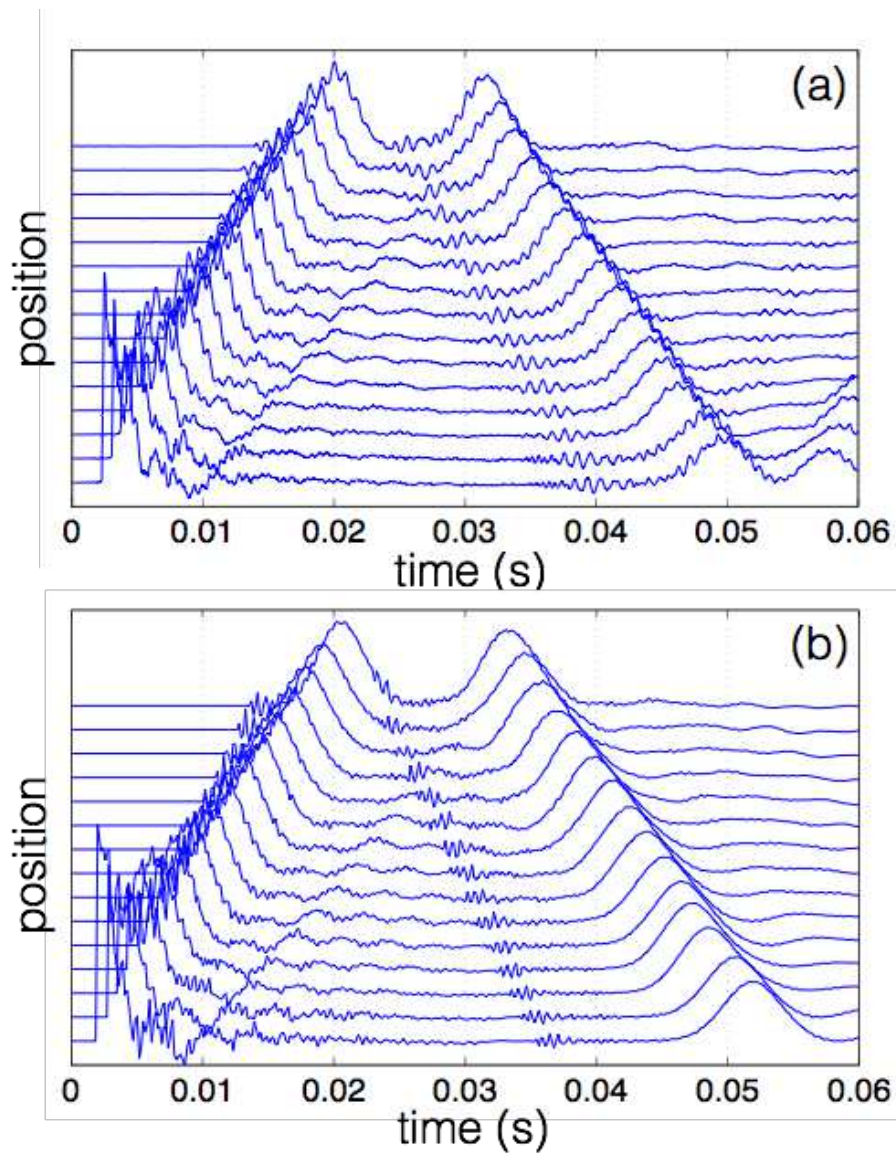


Figure 7: spatio-temporal evolution of the waves in a waveguide with an array of resonators of height  $H = 13$  cm. (a) experiments, (b) simulations. The horizontal axis represents the time  $t$ .

373 *6.3. Attenuation*

374 Figure 8 illustrates the attenuation of acoustic solitary waves during their  
 375 propagation, in the case of resonators with height  $H = 13$  cm. Experimen-

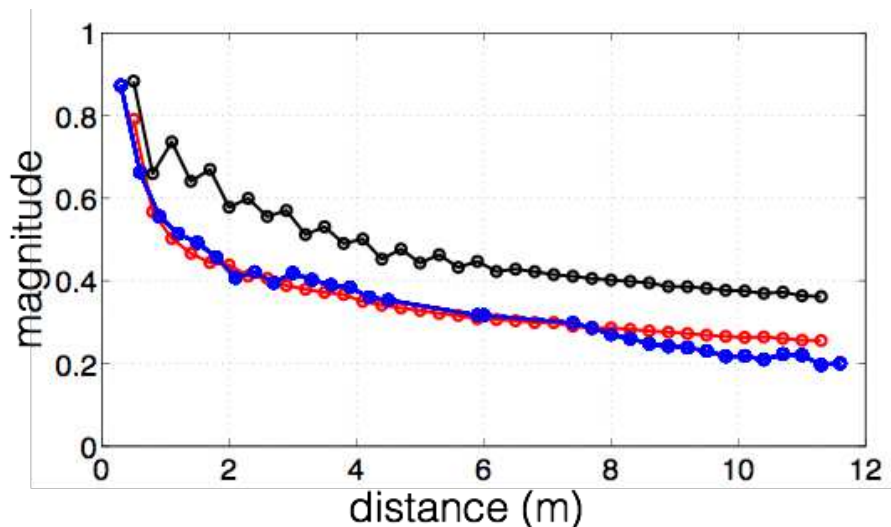


Figure 8: magnitude of the solitary wave in terms of the propagation distance in the lattice, with Helmholtz resonators of height  $H = 13$  cm. Blue line presents the experimental results. Red and black lines present the numerical results obtained with the full model (red) and without the nonlinear attenuation (black).

376 tal results are shown in blue line, and simulated results are shown in red  
 377 and black lines. The red line has been computed by incorporating all the  
 378 mechanisms of attenuation (in particular the nonlinear attenuation in the  
 379 neck), whereas the black line incorporates only the linear viscothermic losses  
 380 ( $m = n = 0$  in (3b)). All these results are deduced from the experimental  
 381 and simulated data presented in the previous section. Good agreement be-  
 382 tween experiments and simulations is obtained when the nonlinear absorption  
 383 processes are taken into account.

384 The evolution of the attenuation in terms of the distance highlights two  
 385 regimes in the wave propagation: a strong attenuation during the first 2  
 386 meters (50 %), followed by a weaker attenuation during the remaining prop-  
 387 agation. Two different mechanisms are involved in the attenuation process  
 388 to explain this observation. Firstly, the nonlinear absorption taking place in  
 389 the resonators is preponderant during the first meters, due to the high am-  
 390 plitude of the initial pulse, which leads to a strong decrease. Secondly and  
 391 owing to the weaker amplitude, the cumulative effects of linear losses during  
 392 the propagation prevails, resulting in a lower attenuation. These mechanisms

393 are deduced from the simulations without the nonlinear absorption: in the  
 394 first regime, the attenuation is largely underestimated while for the second  
 395 regime the slope of the decay is well found.

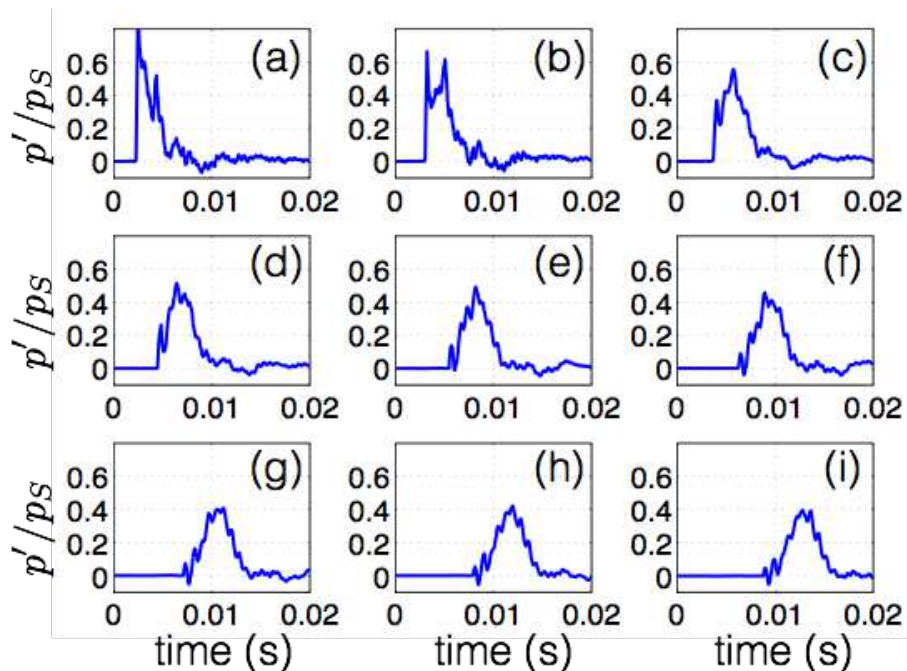


Figure 9: time history of the excess pressure  $p'/p_s$  measured experimentally in the case of Helmholtz resonators of height  $H = 13$ . The measures are done from  $x = 0.2$  m to  $x = 2.6$  m, with a spacing 0.3 m.

396 To highlight these two different regimes, figure 9 shows the time evolution  
 397 of the wave recorded during the first 3 meters. The shape of the initial high  
 398 amplitude pulse is greatly modified, leading to a symmetrical and smooth  
 399 shape after 2 m of propagation. In addition, a strong attenuation is observed  
 400 (50 % of amplitude decay). After, the wave shape remains constant and the  
 401 attenuation becomes weaker. Again, these results show the crucial role of  
 402 nonlinear absorption process in the evolution of a high amplitude pulse to a  
 403 solitary wave.

#### 404 6.4. Influence of the dispersion

405 Here we study the influence of the Helmholtz resonance frequency on the  
 406 features of the solitary waves (velocity, amplitude and shape). Experimental

407 and simulated time evolutions of  $p'/p_s$  are compared in figure 10 in the case  
 408 of heights  $H = 2$  cm (figure 10-(a)) and  $H = 16.5$  cm (figure 10-(b)). Three  
 409 waves are observed from the left to the right, corresponding successively to  
 410 the direct wave at the receivers  $x = 2.8$  m and  $5.95$  m, and to the reflected  
 411 wave at  $x = 2.8$  m. In the case  $H = 2$  cm ( $f_0 = 1027$  Hz), the dispersion is  
 412 weak in the frequency range of the source (see figure 4), contrary to the case  
 413  $H = 16.5$  cm ( $f_0 = 345$  Hz) where the dispersion is strong. Comparing these  
 414 two cases shows the essential role of the dispersion on the characteristics of  
 415 the wave.

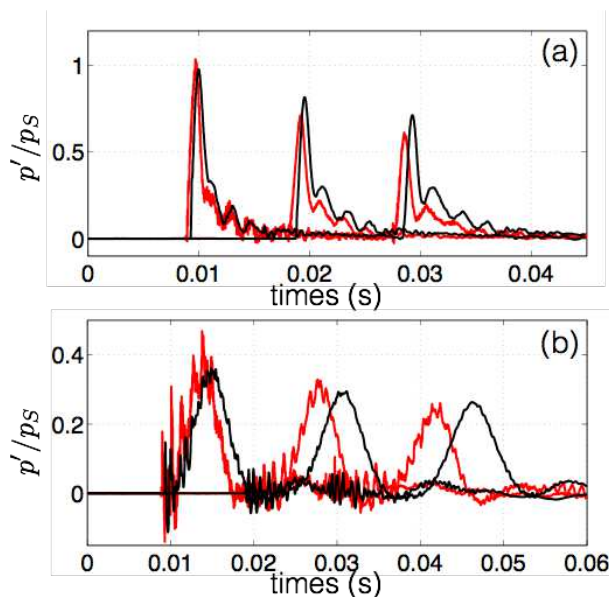


Figure 10: time history of the excess pressure  $p'/p_s$  at  $x = 2.8$  m and  $x = 5.95$  m. (a)  $H = 2$  cm, corresponding to  $f_0 = 1027$  Hz. (b)  $H = 16.5$  cm, corresponding to  $f_0 = 345$  Hz.

416 Weak dispersion combined with nonlinear propagation (figure 10-(a))  
 417 leads to a narrow, compact and less attenuated solitary wave with a high  
 418 velocity. In this case, the velocity and the shape are well recovered by the  
 419 simulation. For strong dispersion (figure 10-(b)), the wave is more attenuated  
 420 and its shape becomes larger. The simulated half-width and the amplitude  
 421 of the wave are in good agreement with the experimental ones. However, a  
 422 slight shift of the positions of waves is observed.



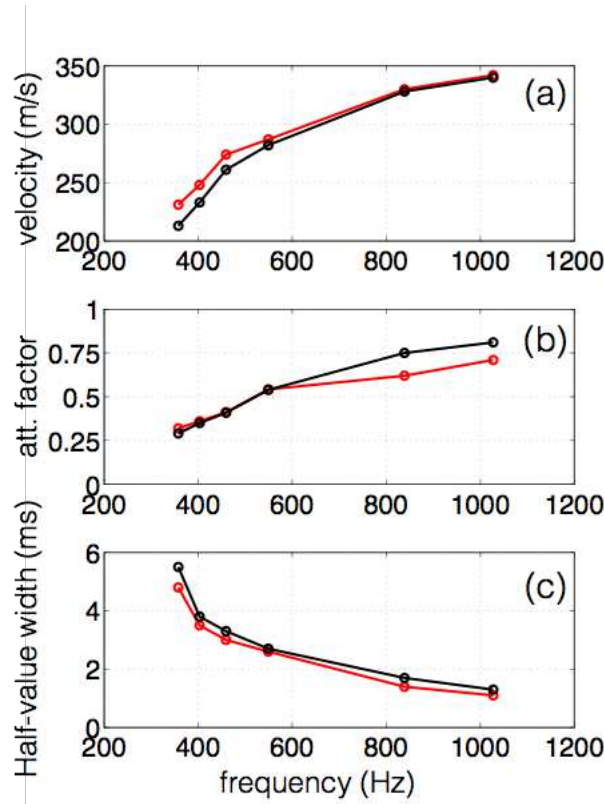


Figure 11: (a) velocity, (b) attenuation factor and (c) half-width of the pulse versus resonance frequencies of the resonators. Experimental and numerical results are shown in red line and black line, respectively.

423 A systematic study is then performed by considering six cavity heights:  
 424  $H = 2, 3, 7, 10, 13, 16.5$  cm. The experimental and simulated excess pressure  
 425  $p'$  is measured at  $x = 2.8$  m and  $5.95$  m in the lattice. The velocity is deduced  
 426 from the traveltime of the maximum of the wave. The attenuation factor is  
 427 given by the ratio of the maximum amplitudes at the two receivers. The  
 428 shape is characterized by the half-width of the solitary wave at  $x = 5.95$  m.

429 All the results are displayed in the figure 11-(a,b,c), where the experi-  
 430 mental results and the numerical results are shown in red and black line,  
 431 respectively. Experiments and simulations are in good agreement, denot-  
 432 ing the good description of the physics by the model and the efficiency of  
 433 the numerical method. As expected, the features of the solitary wave are

434 highly dependent on the Helmholtz resonance frequencies. High resonance  
435 frequency (small  $H$ ) yields large velocity, low attenuation (attenuation fac-  
436 tor close to 1) and narrow wave. The velocity of the wave is close to the  
437 sound speed. For low resonance frequency, conversely, the velocity decreases  
438 and the attenuation and the width of the wave increases. These observations  
439 confirm the main properties of the solitary waves, theoretically analyzed in  
440 [58].

## 441 7. Conclusion

442 We have studied numerically and experimentally the propagation of high  
443 amplitude pulses in a lattice of Helmholtz resonators. We have proposed  
444 a new time-domain numerical method to describe the linear viscothermic  
445 losses in the waveguide and the nonlinear absorption due to the acoustic jet  
446 formation in the necks of resonators. The comparisons between numerical  
447 and experimental results has validated the theoretical model (3) proposed  
448 by Sugimoto, as long as the dissipation processes are correctly incorporated.  
449 Two different regimes of propagation have been observed. Firstly, a strong  
450 attenuation regime, dominated by the nonlinear absorption process, reduces  
451 largely the amplitude of waves and reshapes the acoustic pulses to generate  
452 a solitary wave. Secondly, linear losses in the waveguide produce a lower  
453 mitigation of the solitary wave leading to an almost-constant shape.

454 The properties of the acoustic solitary waves have been studied in terms  
455 of the dispersion of the lattice. In the case of low dispersion, the solitary wave  
456 is compact with a narrow shape. Its velocity is close to the sound celerity  
457 and its attenuation is weak. In the case of a strong dispersion, the shape  
458 of the solitary wave is broader, its velocity is smaller and its attenuation is  
459 large.

460 The numerical and the experimental studies show the great importance  
461 of losses in the generation of acoustic solitary waves in periodic locally reso-  
462 nant structures. It contributes to promising research in the field of nonlinear  
463 acoustic propagation in metamaterials and acoustic transmission filters. Fu-  
464 ture works will be devoted to the study of nonlinear acoustic propagation  
465 in disordered systems. In particular, our numerical and experimental set-  
466 ups will be used to investigate the competition between nonlinear dynamics,  
467 dispersion processes and disorder effects.

468 **Acknowledgments.** This study has been supported by the Agence Na-

469 tionale de la Recherche through the grant ANR ProCoMedia, project ANR-  
470 10-INTB-0914.

- 471 [1] J. R. APEL, L. A. OSTROVSKY, Y. A. STEPANYANTS, J. F. LYNCH,  
472 *Internal solitons in the ocean and their effect on underwater sound*, J.  
473 *Acoust. Soc. Am.*, 121-2 (2007), 695-722.
- 474 [2] M. DE BILLY, A. C. HLADKY-HENNION, *On the formation of envelope*  
475 *solitons with tube ended by spherical beads*, *Ultrasonics*, 52 (2012), 851-  
476 860.
- 477 [3] M. DE BILLY, A. C. HLADKY-HENNION, *Generation of transversal*  
478 *envelope soliton in polymeric and wooden rods*, *Ultrasonics*, 54 (2014),  
479 1281-1288.
- 480 [4] A. BEN JAZIA, B. LOMBARD, C. BELLIS, *Wave propagation in a*  
481 *fractional viscoelastic Andrade medium: Diffusive approximation and*  
482 *numerical modeling*, *Wave Motion*, 51 (2014), 994-1010.
- 483 [5] C. BIRK, C. SONG, *An improved non-classical method for the solution*  
484 *of fractional differential equations*, *Comput. Mech.*, 46 (2010), 721-734.
- 485 [6] N. BOECHLER, G. THEOCHARIS, S. JOB, P. G. KEVREKIDIS, M. A.  
486 PORTER, C. DARAIO, *Discrete breathers in one-dimensional diatomic*  
487 *granular crystals*, *Phys. Rev. Lett.*, 104-24 (2010), 244302.
- 488 [7] A. CHAIGNE, J. KERGOMARD, *Acoustique des Instruments de*  
489 *Musique*, Belin (2008).
- 490 [8] W. CHESTER, *Resonant oscillations in closed tubes*, *J. Fluid Mech.*,  
491 18 (1964), 44-64.
- 492 [9] A. P. CHETVERIKOV, W. EBELING, M. G. VELARDE, *Localized non-*  
493 *linear, soliton-like waves in two-dimensional anharmonic lattices*, *Wave*  
494 *Motion*, 48 (2011), 753-760.
- 495 [10] D. R. CHRISTIE, K. J. MUIRHEAD, R. H. CLARKE, *Solitary waves*  
496 *in lower atmosphere*, *Nature*, 293 (1981), 46-49.
- 497 [11] C. COSTE, E. FALCON, S. FAUVE, *Solitary waves in a chain of beads*  
498 *under Hertz contact*, *Phys. Rev. E*, 56-5 (1997), 6104-6117.

- 499 [12] H. H. DAI, Y. HUO, *Solitary waves in an inhomogeneous rod composed*  
500 *of a general hyper elastic material*, Wave Motion, 35 (2002), 55-69.
- 501 [13] C. DARAIO, V. F. NESTERENKO, E. B. HERBOLD, S. JIN, *Tunabil-*  
502 *ity of solitary wave properties in one-dimensional strongly nonlinear*  
503 *phononic crystals*, Phys. Rev. E, 73-2 (2006), 026610.
- 504 [14] T. DAUXOIS, M. PEYRARD, *Physics of Solitons*, Cambridge Univer-  
505 sity Press (2006).
- 506 [15] K. DIETHELM, *An investigation of some nonclassical methods for the*  
507 *numerical approximation of Caputo-type fractional derivatives*, Numer.  
508 Algor., 47 (2008), 361-390.
- 509 [16] C. M. DONAHUE, P. W. J. ANZEL, L. BONANOMI, T. A. KELLER,  
510 C. DARAIO, *Experimental realization of a nonlinear acoustic lens with*  
511 *a tunable focus*, Appl. Phys. Lett. 104 (2014), 014103 .
- 512 [17] R. J. DOVIAK, S. S. CHEN, D. R. CHRISTIE, *A thunderstorm-*  
513 *generated solitary wave observation compared with theory for nonlinear*  
514 *waves in a sheared atmosphere*, J. Atmos. Sci., 48-1 (1991), 87-111.
- 515 [18] J. ENGELBRECHT, A. BEREZOVSKI, A. SALUPERE, *Nonlinear de-*  
516 *formation waves in solids and dispersion*, Wave Motion, 44 (2007),  
517 493-500.
- 518 [19] J. ENGELBRECHT, V. FRIDMAN, E. PELINOVSKI, *Nonlinear Evolu-*  
519 *tion Equations*, Longman, Harlow (1988).
- 520 [20] B. F. FENG, T. KAWAHARA, *Discrete breathers in two-dimensional*  
521 *nonlinear lattices*, Wave Motion, 45-2 (2007), 68-82.
- 522 [21] B. P. FLANNERY, W. H. PRESS, S. A. TEUKOLSKY, W. T. VET-  
523 TERLING, *Numerical Recipes in C: the Art of Scientific Computing*,  
524 Second Edition, Cambridge University Press (1992).
- 525 [22] M. GRABOWSKI, P. HAWRYLAK, *Wave propagation in a nonlinear*  
526 *periodic medium*, Phys. Rev. B, 41-9 (1990), 5783-5791.
- 527 [23] H. Y. HAO, H. J. MARIS, *Experiments with acoustic solitons in crys-*  
528 *talline solids*, Phys. Rev. B, 64-6 (2001), 064302.

- 529 [24] M. F. HAMILTON, D. T. BLACKSTOCK, *Nonlinear Acoustics*, Aca-  
530 demic Press (1998).
- 531 [25] P. HAWRYLAK, M. GRABOWSKI, *Self-induced gaps and optical bista-  
532 bility in semiconductor superlattices*, Phys. Rev. B, 40-11 (1989), 8013–  
533 8016.
- 534 [26] P. HESS, A.M. LOMONOSOV, *Solitary surface acoustic waves and bulk  
535 solitons in nanosecond and picosecond laser ultrasonics*, Ultrasonics, 50  
536 (2010), 167-171.
- 537 [27] F. KAPPEL, A. KUNTSEVICH, *An implementation of Shor's r-  
538 algorithm*, Comput. Optim. Appl., 15-2 (2000), 193-205.
- 539 [28] Y. V. KARTASHOV, B. A. MALOMED, L. TORNER, *Solitons in Non-  
540 linear Lattices*, Rev. Mod. Phys., 83-1 (2011), 247-305.
- 541 [29] P. G. KEVREKIDIS, *Non-linear waves in lattices: past, present, future*,  
542 IMA J. Appl. Math., 76-3 (2011), 389-423.
- 543 [30] A. S KOVALEV, A. P. MAYER, C. ECKL, G. A. MAUGIN, *Solitary  
544 Rayleigh waves in the presence of surface nonlinearities*, Phys. Rev. E,  
545 66-3 (2002), 036615.
- 546 [31] K. R. KHUSNUTDINOVA, A. M. SAMSONOV, *Fission of longitudinal  
547 strain solitary wave in a delaminated bar*, Phys. Rev. E, 77-6 (2008),  
548 06603.
- 549 [32] S. V. KUZNETSOV, *Soliton-like lamb waves*, J. Appl. Math. Mech., 73  
550 (2009), 71-76.
- 551 [33] A. N. LAZARIDI, V. F. NESTERENKO, *Observation of a new type of  
552 solitary waves in one-dimensional granular medium*, J. Appl. Mech.  
553 Tech. Phys. , 26-3 (1985), 405-408.
- 554 [34] N. LAZARIDES, M. ELEFThERIOU, G. P. TSIRONIS, *Discrete  
555 breathers in nonlinear magnetic metamaterials*, Phys. Rev. Lett., 97-15  
556 (2006), 157406.
- 557 [35] R. J. LEVEQUE, *Numerical methods for conservation laws*, 2nd edi-  
558 tion, Birkhäuser-Verlag (1992).

- 559 [36] Q. LI, C. T. CHAN, K. M. HO, C. M. SOUKOULIS, *Wave propa-*  
560 *gation in nonlinear photonic band-gap materials*, Phys. Rev. B, 53-23  
561 (1996), 15577–1585.
- 562 [37] Q. LI, C. M. SOUKOULIS, S. PNEVMATIKOS, E. N. ECONOMOU,  
563 *Scattering properties of solitons in nonlinear disordered chains*, Phys.  
564 Rev. B, 38-16 (1988), 11888–11891.
- 565 [38] Q. LI, S. PNEVMATIKOS, E. N. ECONOMOU, C. M. SOUKOULIS,  
566 *Lattice-soliton scattering in nonlinear atomic chains*, Phys. Rev. B,  
567 37-7 (1988), 3534–3541.
- 568 [39] Y. LI, F. RAICHLIN, *Non-breaking and breaking solitary wave run-up*,  
569 J. Fluid Mech., 456 (2002), 295-318.
- 570 [40] B. LOMBARD, J.F. MERCIER, *Numerical modeling of nonlinear acous-*  
571 *tic waves in a tube with Helmholtz resonators*, J. Comput. Phys., 259  
572 (2014), 421-443.
- 573 [41] A. M. LOMONOSOV, P. HESS, *Nonlinear surface acoustic waves: Re-*  
574 *alization of solitary pulses and fracture*, Ultrasonics, 48 (2008), 482-487.
- 575 [42] A. P. MAYER, *Nonlinear surface acoustic waves: Theory*, Ultrasonics,  
576 48 (2008), 478-481.
- 577 [43] L. MENGUY, J. GILBERT, *Weakly nonlinear gas oscillations in air-*  
578 *filled tubes; solutions and experiments*, Acta Acustica united with Acus-  
579 tica, 86-5 (2000), 798-810.
- 580 [44] M. MOLERON, A. LEONARD, C. DARAIIO, *Solitary waves in chain of*  
581 *repelling magnets*, J. Appl. Phys., 115 (2014), 184901.
- 582 [45] P. MONKEWITZ, N. M. NGUYEN-VO, *The response of Helmholtz*  
583 *resonators to external excitation. Part 1. Single resonators*, J. Fluid  
584 Mech., 151 (1985), 477-497.
- 585 [46] P. MONKEWITZ, *The response of Helmholtz resonators to external ex-*  
586 *citation. Part 2. Arrays of slit resonators*, J. Fluid Mech., 156 (1985),  
587 151-166.
- 588 [47] I. PODLUBNY, *Fractional Differential Equations*, Academic Press  
589 (1999).

- 590 [48] M. P. RAO, P. CASTRACANE, S. CASADIO, D. FUÀ, G. FIOCCO,  
591 *Observations of atmospheric solitary waves in the urban boundary*  
592 *layer*, Bound.-layer Meteor., 111 (2004), 85-108.
- 593 [49] A. REKIK, R. BRENNER, *Optimization of the collocation inversion*  
594 *method for the linear viscoelastic homogenization*, Mech. Res. Comm.,  
595 38 (2011), 305-308.
- 596 [50] M. REMOISSENET, *Waves Called Solitons: Concepts and Experiments*,  
597 Springer-Verlag, New-York (1999).
- 598 [51] O. RICHOUX, V. TOURNAT, T. LE VAN SUU, *Acoustic wave dis-*  
599 *persion in a one-dimensional lattice of nonlinear resonant scatterers*,  
600 Phys. Rev. E 75 (2007), 026615.
- 601 [52] O. RICHOUX, V. PAGNEUX, *Acoustic characterization of the Hofs-*  
602 *tadter butterfly with resonant scatterers*, Europhys. Lett., 59 (1) (2002),  
603 34-40.
- 604 [53] J. S. RUSSELL, *Report on Waves, Made to the Meetings of the British*  
605 *Association in 1842-1843*, Report of the British Association for the  
606 Advancement of Science, John Murray, London (1844).
- 607 [54] N. SHOR, *Minimization Methods for Non-Differentiable Functions*,  
608 Springer-Verlag (1985).
- 609 [55] N. SUGIMOTO, *Burgers equation with a fractional derivative; heredi-*  
610 *tary effects on nonlinear acoustic waves*, J. Fluid. Mech., 225 (1991),  
611 631-653.
- 612 [56] N. SUGIMOTO, *Propagation of nonlinear acoustic waves in a tunnel*  
613 *with an array of Helmholtz resonators*, J. Fluid. Mech., 244 (1992),  
614 55-78.
- 615 [57] N. SUGIMOTO, T. HORIOKA, *Dispersion characteristics of sound*  
616 *waves in a tunnel with an array of Helmholtz resonators*, J. Acoust.  
617 Soc. Am., 97-3 (1995), 1446-1459.
- 618 [58] N. SUGIMOTO, *Acoustic solitary waves in a tunnel with an array of*  
619 *Helmholtz resonators*, J. Acoust. Soc. Am., 99-4 (1996), 1971-1976.

- 620 [59] N. SUGIMOTO, M. MASUDA, J. OHNO, D. MOTOI, *Experimental*  
621 *demonstration of generation and propagation of acoustic solitary waves*  
622 *in a air-filled tube*, Phys. Rev. Lett., 83-20 (1999), 4053-4056.
- 623 [60] N. SUGIMOTO, M. MASUDA, K. YAMASHITA, H. HORIMOTO, *Verifi-*  
624 *cation of acoustic solitary waves*, J. Fluid. Mech., 504 (2004), 271-299.
- 625 [61] C. E. SYNOLAKIS, *The run-up of solitary waves*, J. Fluid Mech., 185  
626 (1987), 523-545.
- 627 [62] E. F. TORO, *Riemann Solvers and Numerical Methods for Fluid Dy-*  
628 *namics. A Practical Introduction*, Springer-Verlag (1999).
- 629 [63] Y. WAN, C. M. SOUKOULIS, *Wave transmission in one-dimensional*  
630 *nonlinear lattice : multi stability and noise*, Springer Proceedings in  
631 Physics: Disorder and Nonlinearity, 39, Springer-Verlag, Berlin (1989).
- 632 [64] Y. WAN, C. M. SOUKOULIS, *One-dimensional nonlinear Schrödinger*  
633 *equation: A nonlinear dynamical approach*, Phys. Rev. A, 41-2 (1990),  
634 800-809.